Case Studies in Thermal Engineering 49 (2023) 103184

Contents lists available at ScienceDirect

Case Studies in Thermal Engineering

journal homepage: www.elsevier.com/locate/csite

Research on the heat transfer performance of an improved elastic tube bundle heat exchanger under fluid-induced vibration

Jiadong Ji *, Yuling Pan, Xu Deng, Jingwei Zhang, Ping Liu

School of Mechanical Engineering, Anhui University of Science & Technology, Huainan, 232001, China

ARTICLE INFO

Handling Editor: Huihe Qiu

Keywords:
Heat exchanger
Improved planar elastic tube bundle
Fluid-induced vibration
Heat transfer

ABSTRACT

The heat transfer performance (HTP) of an improved elastic tube bundle (IETB) was analyzed using a bi-directional fluid-structure interaction calculation method. The vibration-enhanced HTP of heat exchangers with different inlet velocities (U_{in}) and row number N were studied. The results show that the amplitude gradually increases as the U_{in} increase with a maximum increase of 309.98%. The amplitude with fixed shell side length (FL-heat exchanger) is generally higher than that with variable shell side length (VL-heat exchanger) under different row numbers. The average amplitude of the three directions increased by 4.55%, 11.54%, and 7.41%, respectively. The heat transfer coefficient (h) is directly proportional to U_{in}, and the comprehensive HTP gradually decreases with the increase of U_{in}. With the increase in the row numbers, h generally showed a downward trend. For the VL-heat exchanger, h decreases as the row number increases, which increases from N=6 to N=9, and h decreases by 13.85%. For the FL-heat exchanger, h first increases and then gradually decreases. The comprehensive HTP also maintained the same trend. Compared VL-heat exchanger and FL-heat exchanger, reducing the spacing between tube rows increases heat transfer per unit volume, leading to improved comprehensive HTP of the IETB heat exchanger.

Nomenclature

a	Acceleration($m \cdot s^{-2}$)
A	amplitude (mm)
D	diameter (mm)
f	frequency (Hz)
g	shell side fluid resistance coefficient (-)
H	height (mm)
h	heat transfer coefficient ($W \cdot m^{-2} \cdot K^{-1}$)
i	tube number (-)
k	thermal conductivity ($W \cdot m^{-1} \cdot K^{-1}$)
L	length (m)
N	tube row number (-)
Nu	Nusselt number (-)

* Corresponding author.
E-mail address: jjd1006@163.com (J. Ji).

https://doi.org/10.1016/j.csite.2023.103184
Received 7 May 2023; Received in revised form 7 June 2023; Accepted 10 June 2023
Available online 12 June 2023

$P(p)$	pressure (Pa)
ΔP	pressure drop (Pa)
q	heat flow density ($W{\cdot}m^{-2}$)
R	radius (mm)
R_e	Reynolds number (-)
T	temperature (K)
ΔT	temperature difference (K)
t	time (s)
U	fluid velocity ($m{\cdot}s^{-1}$)

Greek letters

σ	inhomogeneity coefficients
δ	wall thickness (mm)
α	thermal diffusivity (W·m-1·K-1)
v	kinematic viscosity (kg·m-1·s-1)
υ	Poisson's ratio (-)
ρ	density ($kg{\cdot}m^{-3}$)

Subscripts

a	average
F	fluid-solid interface
f	shell-fluid
i	number (-)
in	inlet
out	outlet
v	vibration

Abbreviations

IETB	improved elastic tube bundle
HTP	heat transfer performance

1. Introduction

Heat exchangers [1–3] are commonly used devices for exchanging energy in industries such as aerospace, chemical, and refrigeration production. When the traditional tubular heat exchanger works, its internal rigid heat transfer elements begin to vibrate under the impact of fluid, which can result in fatigue damage and decreased heat exchanger service life [4,5]. Shell and tube heat exchangers [6,7] are currently the most widely used in industrial production. The study of enhanced heat transfer in heat exchangers has become a hot topic of current research [8]. To reduce the influence of fluid shock, utilizing the vibration-enhanced heat transfer principle, an elastic tube bundle heat exchanger is proposed [9,10]. The material of the heat transfer element was replaced from steel to copper to achieve small amplitude vibration of the internal tube bundle at the low frequency, this improvement not only improves the heat transfer coefficient (h), but also uses the vibration deformation to remove the scale on the heat transfer surface, reduce the thermal resistance, and finally realize the composite heat transfer enhancement. However, due to the disadvantages such as poor comprehensive heat transfer performance (HTP) of elastic tube bundles, it is essential to improve the structure to obtain better comprehensive HTP.

Yan et al. [11,12] proposed a conical spiral tube to study its heat transfer characteristics from the aspect of structural parameters. The findings indicate that the angle and section size significantly impact h, and that always remains at about 148 $W{\cdot}m^{-2}{\cdot}K^{-1}$ when the pitch changes. Jiang et al. [13] obtained the local surface h of the tube bundle by establishing a constant heat flow experimental platform for heat exchangers. The outcome reveals that the h was notably superior in the central tube bundles as compared to the tubes at the periphery. Moreover, the h value at the free end was slightly superior to that of other locations. Ji et al. [14–16] created a platform to test the vibration response for planar elastic tube bundles using a shell side distributed pulsating flow generator to induce fluid flow. The results show that the vibration intensity of each row is the same, and there is an obvious "double peak" phenomenon in its vibration. Duan et al. [17,18] conducted an in-depth study on the mechanism of enhanced heat transfer of the tube bundle using field synergy theory. The results show that the two key factors of enhanced heat transfer are the improvement of the field synergy effect and the relative speed of oscillation. Among them, the leading role in enhancing heat transfer is to improve field synergy. In addition, the pressure drop and heat transfer characteristics became more stable when pulsating flow frequency was increased. Ji et al. [19,20] proposed the improved elastic tube bundle (IETB) by separating the mass block, and studied and compared the HTP under varying U_{in}. The findings show that the HTP of IETB is increased by 8.44%, 6.91%, 5.50%, and 2.41% respectively compared to traditional elastic tube bundles [16] at U_{in} of 0.1–1.0 m/s. However, performance studies of heat exchangers with different rows of IETBs are lacking at this stage. Gugulothu [21,22] investigated the effect of segmented baffles on the performance of shell and tube heat exchangers. The results show that the variation in baffle spacing has a significant effect on the turbulence and heat transfer performance of the heat

exchanger, with the heat transfer performance improving as the baffle spacing decreases. Kaleru [23,24] investigated the performance of heat exchangers with segmented baffles and spiral baffles with different inclination angles. The results show that the 40° spiral baffle has a higher performance than the segmented baffle and the 20° and 30° spiral baffle heat exchangers.

Due to the advantages of IETB in terms of vibration-enhanced HTP, combined with the IETB heat exchanger structure, the influence of different U_{in} and different row numbers on the vibration-enhanced HTP of the heat exchanger was researched. The performance of the heat exchanger under different conditions is analyzed based on different options for increasing or decreasing the number of rows, to obtain the optimal performance solutions.

2. Models and method

2.1. Structural domain

Fig. 1 is a schematic diagram of the heat exchanger structure. Fig. 1 illustrates the IETBs are uniformly aligned and fixed on horizontal tubes, each containing four curved copper tubes as well as three mass blocks. Different from the previous structural model, the IETB adopted in this paper uses two small mass blocks (mass blocks A and B) to replace the original large mass block, which can reduce their natural frequency and enhance their low-speed vibration characteristics [20]. The structural design parameters of the IETB and the mass blocks A, B, and C within the bundle are marked (corresponding values are shown in Table 1). The heat exchanger operates with the high-temperature tube side fluid entering through the left “Tube side inlet”, flowing through each tube bundle successively, and leaves from the right “Tube side outlet”; The low-temperature shell side fluid entering through the “Shell side inlet”, exchanges heat with IETBs, and exits through the upper “Shell side outlet".

2.2. Fluid domain

Considering that the IETB vibration is mainly caused by the shell side fluid [19,20], the fluid domain investigated in this paper is shown in Fig. 2.

To analyze how the row number change of IETB affects its vibration-enhanced heat transfer., there are two methods for altering the tube row count, so, the heat exchanger model is defined as a fixed shell side length heat exchanger (FL-heat exchanger) and variable shell side length heat exchanger (VL-heat exchanger) under different numbers of tube rows. The IETBs are fixed on the two horizontal tubes with the same spacing H. For the FL-heat exchanger, the shell side length L_f is constant and the spacing H_f is variable, the number of tube rows can be varied by changing the value of H_f. For the VL-heat exchanger, the spacing H_v is constant, and the shell side length L_v increases with the number of tube rows. To facilitate analysis, IETBs are numbered as i (i=1, 2, 3 … 7, 8, 9) from right to left. So, monitoring points A_i, B_i, and C_i are set on mass blocks A, B, and C to record the vibration displacement of the mass blocks and detect the vibration of IETBs. Table 1 displays the structural parameters specified in this paper.

2.3. Grids and boundary conditions

In Fig. 3, the mesh for both the fluid and structural domains is displayed. (9 rows of IETB of VL and FL-heat exchanger), this type of computational model has the largest number of grids. The fluid domain and mass blocks of IETBs adopt tetrahedral mesh, while the IETB curved copper tubes in the structural domain adopt hexahedral mesh. To improve the accuracy of numerical results, a 10-layer boundary is added to the fluid-structure interaction wall. The structural domain consists of 29730 elements and 125682 nodes. Under the different categories of heat exchangers, the element and node number of the fluid domain is shown in the following Table 2.

The boundary conditions are set as the followings: The direction of gravitational acceleration is –y direction with the value of 9.81 m/s^2. Both ends of IETB are defined as “Fixed Support”, while the outer surface is defined as a “Fluid Solid Interface”. In the fluid domain, the two ports are defined as “Inlet” and “Outlet”, where the temperature loading on the inlet T_{in} is 293.15K. and the relative outlet pressure P_{out} is 0 Pa. The “Velocity” of “Inlet” is set as 0.1–0.7 m/s (value of U_{in}), Combined with U_{in}, the Reynolds number R_e is calculated to be in the range 1000–7000, due to the local turbulence that forms around the tube bundle when the R_e is small. So, the standard k-ε model is employed for calculating shell side fluid [20]. And the fluid internal walls corresponding to the structural domain are set as “Fluid Solid Interface”, and its temperature T_F is 333.15 K. In addition, the horizontal tube and fluid domain boundary walls are provided with no slip and adiabatic walls.

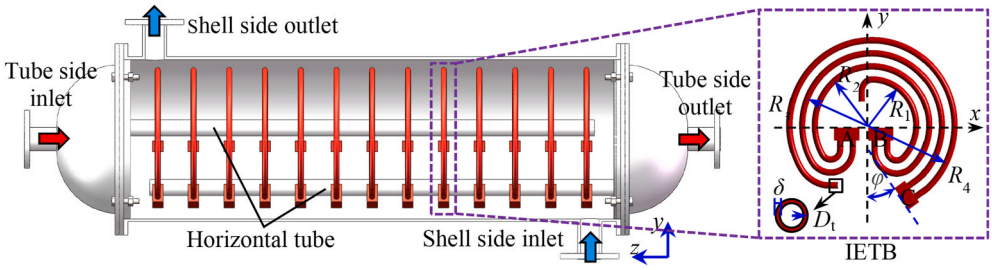

Fig. 1. IETB heat exchanger.

Table 1
Structural parameters.

Category	Parameters	Values
Shell side domain	Diameter D/mm	300
	Entrance diameter D_{in}/mm	34
	Exit diameter D_{out}/mm	34
VL-heat exchanger	Length L_v/mm	540, 630, 720, 810
	Spacing H_v/mm	90
FL-heat exchanger	Length L_f/mm	630
	Spacing H_f/mm	67.5, 77, 90, 108
Copper tube properties	Bending radius R_1, R_2, R_3, R_4/mm	70, 90, 110, 130
	Section radius D_t/mm	5
	Wall thickness δ/mm	1.5
	Density ρ_c/kg · m^{-3}	8900
	Elastic modulus/Pa	1.29×10^{11}
Mass block properties	Length, width, and height l_b, w_b, h_b/mm	40, 20, 20
	Density ρ_b/kg · m^{-3}	7800
	Elastic modulus/Pa	2.10 × 10^{11}

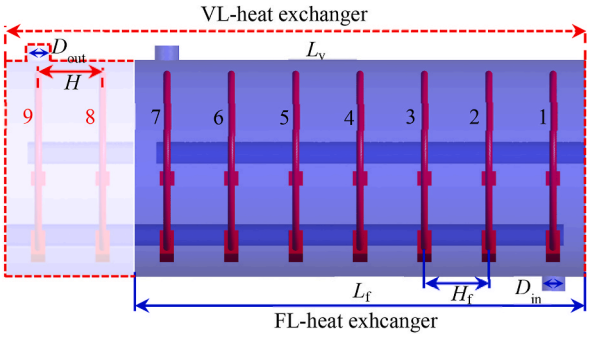

Fig. 2. The fluid domain of the IETB heat exchanger.

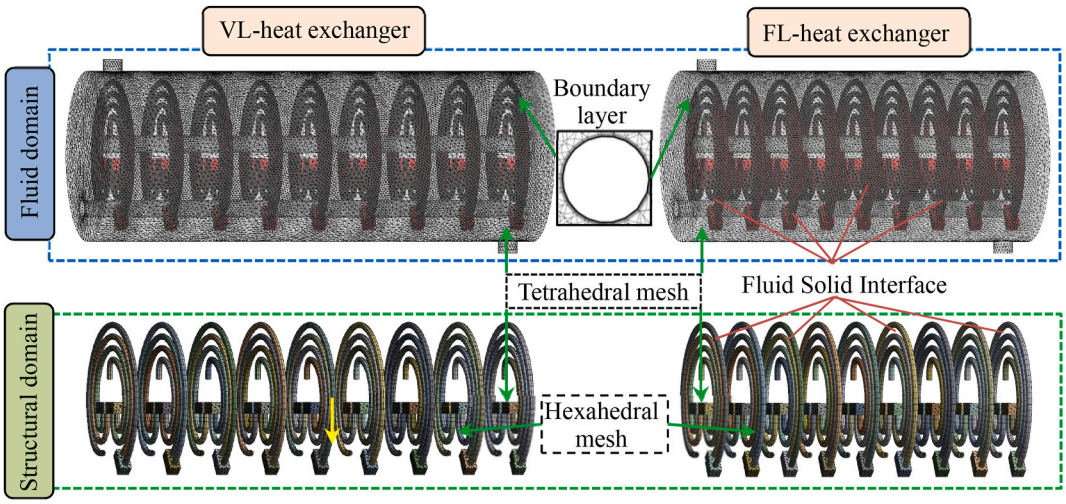

Fig. 3. Mesh division of fluid domain and IETBs.

2.4. Calculation method

In fluid domain calculation, without considering heat loss, the steady-state equations can be as follows [10,20]:
Continuity equation

$$\nabla \cdot U = 0 \tag{1}$$

Table 2
Mesh and node number of the fluid domain.

Category	Length/mm	Elements	Nodes
VL	810	10471500	1907540
FL	630	10354002	1883032

Momentum equation

$$(U \cdot \nabla)U = -\frac{1}{\rho}\nabla P + v\nabla^2 U \tag{2}$$

Energy equation

$$(U \cdot \nabla)T = \alpha\nabla^2 T \tag{3}$$

where the equation involves the variables of fluid velocity (U), pressure (P), temperature (T), kinematic viscosity (v), and thermal diffusivity (α).

In the fluid that needs a certain time to flow fully in the IETB heat exchanger, this paper uses the method of conducting an initial calculation followed by an actuarial calculation [16]. The initial calculation is 300s and the time step is 0.1s to make the fluid reach a steady state, the actuarial calculation is 1.2s with a time step is 0.001s. Fig. 4 illustrates the detailed calculation process.

Fig. 4 depicts the computational procedure for modeling the bi-directional fluid-structure interaction, which was performed using the ANSYS and CFX software. Firstly, the geometry models of the fluid and structure domain adopted in this paper are established. Then the grid of the geometry models is divided by the "Mesh". The CFX solver is used for the initial computation to obtain the data and initial force on the tube surface, which will be used as the initial conditions for the structural calculation. Finally, actuarial calculations begin by connecting the ANSYS and CFX software. CFX solver calculates the force on the tube bundle surface, then transmits it to ANSYS solver through the "Fluid Solid Interface". The latter, after solving the vibration equations, transmits the tube bundle displacement to the CFX solver for calculating the surface force under the new grid boundary. This loop continues until the calculation is complete.

2.5. Verification of grid and numeric codes

To ensure accurate and efficient simulation results, the grid independence analysis of the IETB heat exchanger (N=9) was studied (shown in Fig. 3), and Table 3 illustrates the grid independence verification results. By reducing and increasing the number of elements, both the calculated outlet temperature (T_{out}) and the h of the same IETB were recorded and compared.

As can be seen from Table 3, compared category I and II, the maximum relative error is 5.71% in h, and the time increased by nearly double. Compared the II and III, the maximum relative error is 1.83%, and the time increased by 162%. Increasing the number of grids can get more accurate calculation results but can also lead to a reduction in calculation efficiency. To balance accuracy and efficiency, this paper adopts the grid classification method in category II.

To verify the reliability of numerical methods, the identical computational model as in the literature [16] was established, and the grid division method described previously was used. After calculating numerical results, the vibration frequencies f and accelerations a of monitoring point M_1 and N_1 on the elastic tube bundle at V_{in} = 0.4 m/s comparison with experimental data were analyzed and shown in Table 4. The relative errors in f and a on M_1 are 2.92% and 1.88%, respectively; On the N_1, the errors are 1.92% and 1.94%, respectively. All of them are less than 5.00%. So, the numerical calculation method used is reliable.

Adopted the above boundary conditions and numerical method to calculate the h of the coiled tube in the reference [25]. Fig. 5 shows the comparison between the formula and simulation results. As can be seen from Fig. 5, the simulation results are very consistent

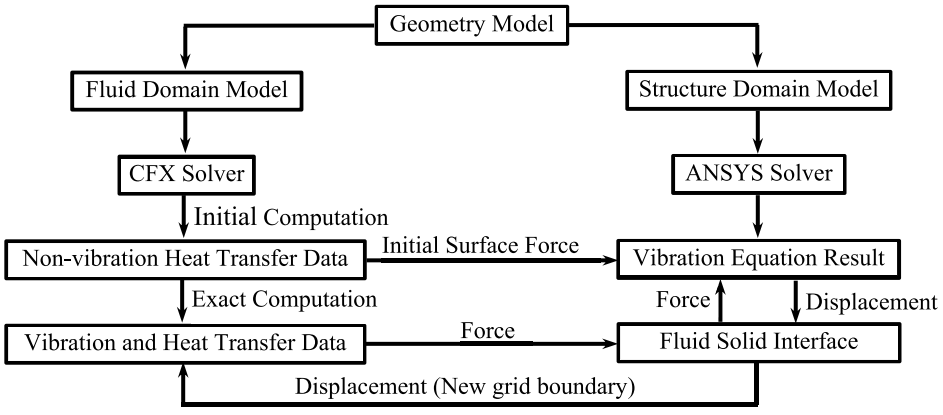

Fig. 4. Detailed calculation process.

Table 3
Grid independence analysis.

Category	Elements	Simulation results		Relative error, %		Computing time/h
		T_{out} /K	h/W·m^{-2}·K^{-1}	T_{out}	h	
I	8,795,922	288.19	437.15	3.08	5.71	51
II	10,471,500	297.34	463.62	–	–	114
III	12,801,458	299.45	472.10	0.71	1.83	185

Table 4
Comparison of results.

Results	f/Hz		a/m·s^{-2}	
	M_1	N_1	M_1	N_1
Experimental data [16]	24.0	26.0	1.117	0.567
Numerical results	24.7	26.5	1.132	0.578
Relative error	2.92%	1.92%	1.88%	1.94%

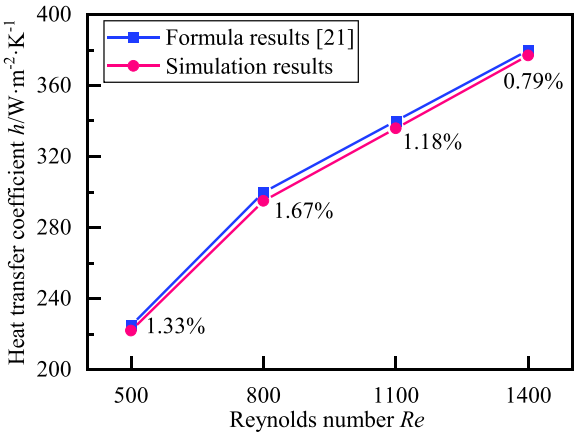

Fig. 5. Validation of numerical calculation method.

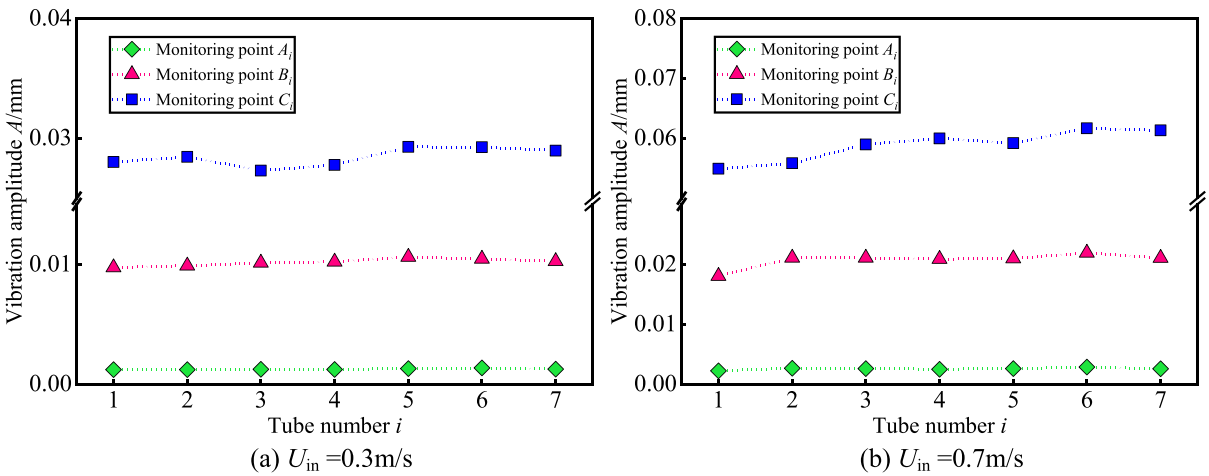

Fig. 6. Amplitude changes at each monitoring point.

with the empirical formula results, with a maximum relative error of 1.67%, indicating that the numerical method used is convincing.

3. Vibration characteristics analysis

3.1. Effect of inlet velocity

According to the numerical simulation on the IETB heat exchanger with different U_{in} (tube row number N=7, and tube row spacing H=90 mm corresponds to the heat exchanger in Ref. [20]), the effect of U_{in} on IETB vibration characteristics was studied. To compare the vibration characteristics of each IETB, the Fourier transform of the vibration displacement data of different monitoring points was performed to obtain the vibration amplitude (A) changes of the total displacement directions of each monitoring point A_i, B_i, and C_i at different U_{in} (0.3, 0.7 m/s), and the results are shown in Fig. 6.

It is easy to see from Fig. 6 that the amplitudes of each monitoring point of IETB 1-IETB 7 do not differ much under different U_{in}, and the fluctuation of monitoring point C_i is the largest. At the same U_{in}, the amplitudes of monitoring points C_1-C_7 are the largest, followed by monitoring point B_i, and A_i is the smallest. With the increase of U_{in}, the change of monitoring point C_i is more obvious and the vibration is intense, and the influence on monitoring points A_i, B_i is smaller. So, the subsequent study of the vibration characteristics of IETBs could justifiably employ the vibration taken at monitoring point C_i as a representative.

To investigate the vibration characteristics of IETBs, the displacement data in different directions of monitoring point C of IETB 4, which is in the middle position of the heat exchanger, is Fourier transformed to observe the vibration intensity changes of IETBs in different directions, and the spectrum plots at different U_{in} were obtained, as shown in Fig. 7.

As can be seen from Fig. 7,

(1) At different U_{in}, the amplitude changes with frequency in the three directions are the same. With the increase in frequency, the amplitude increases first and then decreases gradually after reaching the peak value. In addition, the z direction differs from other directions in that there is no turning point at 20.2 Hz.
(2) U_{in} does not affect the main vibration frequency in different directions. At each U_{in}, the main vibration frequency in all directions is 16.84 Hz.
(3) When U_{in} is 0.3 m /s, the amplitude is maximum in the x direction, followed by the y direction, and minimum z direction, which suggests the predominantly in-plane vibration when U_e is low. As the U_{in} increases, the force enhances, so the amplitude of the primary impact direction (z direction) of the fluid increases significantly. The amplitude at 0.7 m/s is 7.62 times greater than at 0.3 m/s. In this case, the amplitude with the z direction is greater than the other directions, which suggests the predominant vibration is out-of-plane at high U_{in}.

The average amplitudes (A_a) of monitoring points C_1-C_7 at different U_{in} were calculated to reflect the overall vibration intensity of 7 rows of IETBs. Meanwhile, the vibration inhomogeneity coefficients σ_v of 7 rows of IETB were calculated to reflect the z-vibration uniformity of IETBs by the following equations (4) and (5). The results are shown in Fig. 8.

The average amplitude A_a and vibration inhomogeneity coefficients σ_v is calculated as follows:

$$Aa = \frac{1}{n}\sum_{i=1}^{n} Ai \tag{4}$$

$$\sigma_v = \sqrt{\frac{1}{n}\sum_{i=1}^{n}\left(\frac{A_i - Aa}{Aa}\right)^2} \tag{5}$$

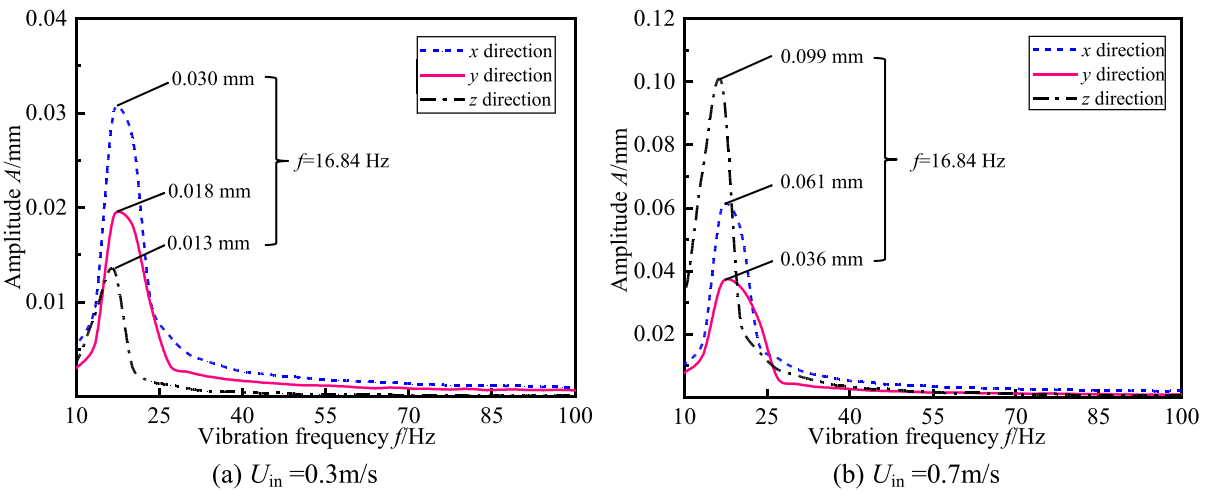

Fig. 7. Vibration spectrum of the IETB 4.

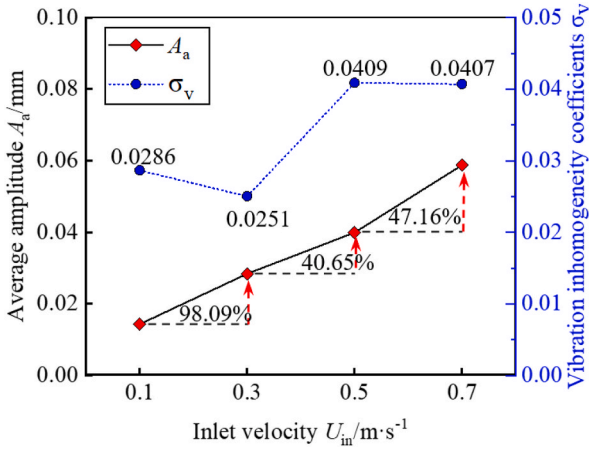

Fig. 8. Average amplitude A_a and vibration inhomogeneity coefficients σ_v with U_{in}.

It is evident from Fig. 8,

(1) The amplitude of the IETBs increases as the U_{in} increases. When the U_{in} increased from 0.1 m/s to 0.7 m/s, the amplitude increased by 309.98%. So, increasing the U_{in} has a positive effect on enhancing the IETB vibration intensity.
(2) The vibration inhomogeneity coefficients of IETBs at different U_{in} are less than 0.05, which indicates that the vibration uniformity of the 7-rows IETBs is better. At U_{in} of 0.1 and 0.3 m/s, the values of σ_v are 0.0286 and 0.0251, respectively, which are small compared with those at 0.5 and 0.7 m/s. This indicates that the vibration uniformity of the 7-rows IETBs is better at low U_{in}.

3.2. *Effect of row number*

Based on the numerical simulation calculation of the IETB heat exchanger under different row numbers *N*, the influence of row number on vibration characteristics was studied and analyzed. As Fig. 2 shows, the row numbers *N* studied in this paper are 6, 7, 8, and 9 separately. Due to the difference in approach, there are two categories, VL and FL-heat exchanger. The amplitude variation of C_i of IETBs in different directions is calculated for different categories when U_{in} is 0.5 m/s.

It is evident from Fig. 9.

(1) For the VL-heat exchanger, vibration in different directions shows an increasing trend as a whole. The amplitudes of the third and seventh rows are slightly higher than the others. This is because the third row is located at the junction of the inlet part and the middle part. The flow velocity of the surrounding fluid is higher. Based on prior research [20], the higher the U_{in}, the greater the fluid impact force. Therefore, the amplitude of IETBs has been improved. For the same reason, the amplitude of the seventh row is the largest in different directions.
(2) For the FL-heat exchanger, the amplitude of IETBs in different directions increases first, reaches the maximum at the IETB 8, and decreases sharply at the IETB 9. The reason for this tendency is that because the tube row is particularly dense, part of the fluid

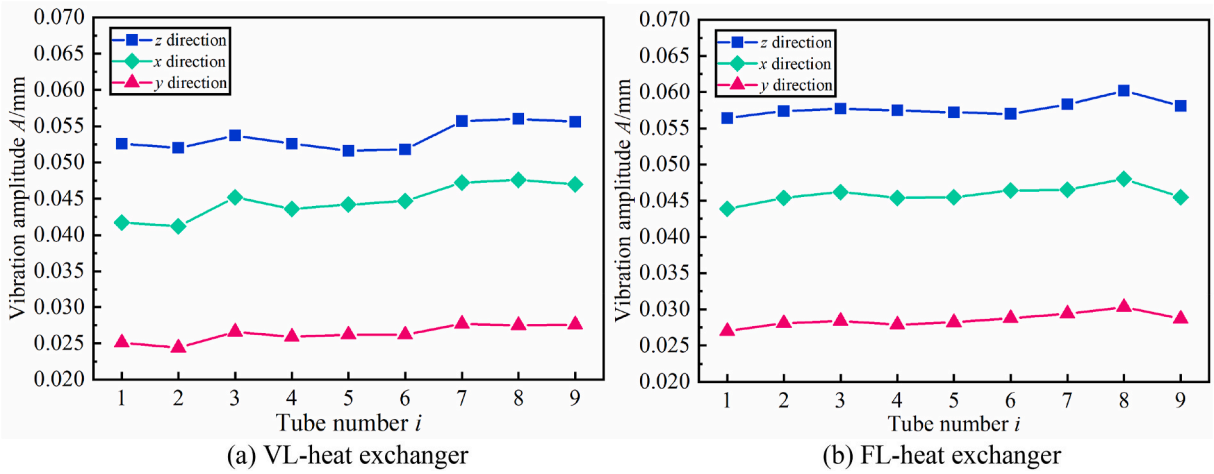

Fig. 9. Variation of IETBs amplitude in different directions.

flows through the 8th row and directly into the outlet from the upper left. This weakens the force between the fluid and the 9th-row IETB, so the amplitude of the last row decreases sharply. Different from the conclusion (1), the amplitude of the IETB 3 and IETB 7 is not significantly higher than those of the peripheral bundles, which is also related to the flow domain distribution. At this time, the spacing of tube rows is very small (only 67.5 mm), resulting in a more uniform flow domain distribution than the large spacing (90 mm), the third and seventh rows of tube bundles received the same fluid impact force as other IETBs. Therefore, as shown in Fig. 9 (b), the amplitude of different rows of tubes in the same direction differs little.

(3) By comparing Fig. 9 (a) and (b), it can be seen that the amplitude of IETBs in the FL-heat exchanger is generally higher than the VL-heat exchanger. For the former, the average amplitude in the different directions is 0.044 (x), 0.026 (y), and 0.054 (z) mm, respectively. For the latter, the average amplitudes in the three directions are 0.046 (x), 0.029 (y), and 0.058 (z) mm, separately, increasing by 4.55%, 11.54%, and 7.41%. This is because the vortex shedding of the front tube bundle is easier to act on the back row as the row spacing decreases. Therefore, the vibration effect of IETBs is better in the FL-heat exchanger.

To investigate the overall vibration characteristics of the IETBs, the average amplitude A_a was calculated. Fig. 10 manifests the A_a of IETBs in the VL and FL-heat exchanger.

It is evident from Fig. 10,

(1) For the VL-heat exchanger, the row spacing is constant and the row number is increased, A_a decreases gradually, indicating that the shell side length is excessively raised with the increase of row number, which will weaken the interaction of the fluid and IETBs.

(2) For the FL-heat exchanger, A_a decreases first and then increases, especially since the A_a of the nine-row IETB heat exchanger is larger than that six-row. This is because the distance between the rows of tubes is greatly reduced. Consistent with the previous conclusion, the force between the fluid and IETBs is enhanced, so the average amplitude increases significantly. Similarly, for two kinds of heat exchangers with shell side lengths, while the row number is constant, A_a with small spacing is always higher than A_a with large spacing. When the length of the nine-row IETB heat exchanger is fixed, the spacing decreases by 22.5 mm, while the amplitude increases by 12.97%.

4. Heat transfer performance

4.1. Effect of inlet velocities

Based on the numerical simulation in the heat exchanger with various U_{in}, its HTP was studied. Initial conditions are N=7 and H=90 mm h and h_v indicate the heat transfer coefficients under the absence and presence of vibration (the subscript "v" indicates the vibration condition), respectively. Fig. 11 shows the h and h_v of each IETB at different U_{in}.

The formula for h is as follows:

$$h = \frac{q}{\Delta T} \tag{6}$$

where q represents heat flow density, the log-average temperature difference (ΔT) is calculated as follows:

$$\Delta T = \frac{T_{out} - T_{in}}{\ln[(T_{in} - T_F)/(T_{out} - T_F)]} \tag{7}$$

It is not difficult to see from Fig. 11, each IETB achieves enhanced heat transfer by vibration at different U_{in}. Since the larger the fluid U_{in} is, the stronger its turbulence, the h/h_v of IETB is significantly higher at high U_{in} than at low U_{in}. At the same time, the h and h_v increase differently. When U_{in}=0.1 m/s, vibration-enhanced heat transfer is better, and the maximum increase (h_v-h)/h reaches 21.03%. While U_{in}=0.7 m/s, the increase is significantly lower, with a maximum increase of only 6.87%.

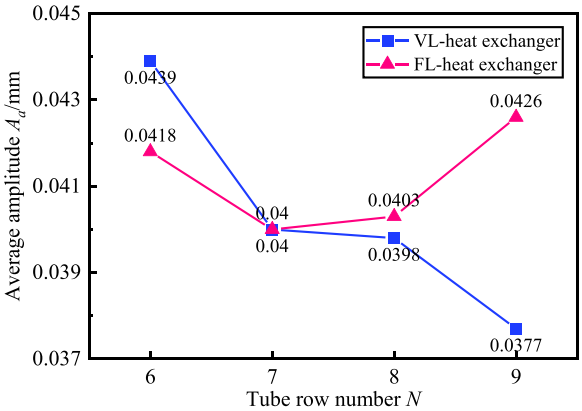

Fig. 10. Variation of average amplitude with row numbers.

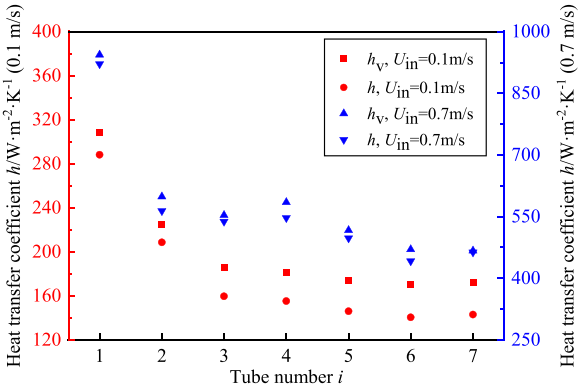

Fig. 11. Influence of inlet velocities U_{in} on h/h_v of IETB.

To visually analyze the variation of HTP with U_{in}, the average heat transfer coefficient (h_a/h_{va}) of IETBs at different U_{in} was calculated to reflect the HTP of IETBs, as Fig. 12 shows. (The subscript "a" indicates the average value, h_{va} represents the average h_v under vibration conditions.) The equation for h_a is as follows:

$$h_a = \frac{1}{n}\sum_{i=1}^{n} h_i \tag{8}$$

It is easy to see from Fig. 12,

(1) The h_a of IETBs is proportional to U_{in}. When the value of U_{in} rises from 0.1 to 0.7, h_a improves by 220.06% and h_{va} improves by 183.45%. This is since the average thickness in the boundary layer decreases as the fluid turbulence intensity increases.
(2) h_{va} is always greater than h_a, and when U_{in}=0.1 m/s-0.7 m/s, the enhancement is 17.48%, 8.43%, 5.58%, and 4.02% compared to h_{va} and h_a, respectively. This indicates that the vibration-enhanced heat transfer is stronger under lower U_{in}.

The Performance Evaluation Criteria (*PEC*) tends to evaluate the comprehensive HTP for IETB heat exchangers [26]. It indicates that the heat exchanger achieves enhancing heat transfer while the *PEC* value is over 1.00, and its specific expression is as follows:

$$PEC = (Nu_v / Nu) \Big/ (f_v/f)^{1/3} \tag{9}$$

$$Nu = \frac{hD_t}{k} \tag{10}$$

The fluid resistance coefficient is calculated by the following formula [27]:

$$f = \frac{2\Delta P D_t}{H\rho U_a^2} \tag{11}$$

where thermal conductivity (k) and average fluid velocity (U_a) are included.

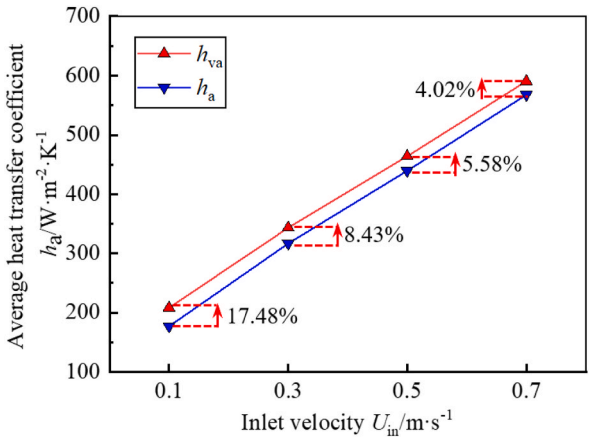

Fig. 12. Influence of inlet velocity U_{in} on average h_a/h_{va} of IETBs.

The heat transfer coefficient per unit pressure drop ($h/\Delta P$) is used to represent the comprehensive HTP of the IETB heat exchanger. The variation of $h/\Delta P$, $h_v/\Delta P$, and *PEC* for different U_{in} is shown in Fig. 13 by calculation.

It is evident from Fig. 13,

(1) Both $h/\Delta P$ and $h_v/\Delta P$ decrease as U_{in} increase due to the high-velocity fluid requiring more energy consumption to transport. In addition, after calculation, at the same U_{in}, especially at 0.1 m/s, compared to $h/\Delta P$, $h_v/\Delta P$ increased by 17.47%. When the U_{in} is 0.7 m/s, the $h_v/\Delta P$ increases by only 4.37% to $h/\Delta P$, which further proves that IETB is more accessible to realize vibration-enhanced heat transfer under low U_{in} [28].

(2) *PEC* value decreases gradually with the increase of U_{in}. When U_{in} is 0.1 m/s, the *PEC* value is 1.078, and when the U_{in} is 0.5 m/s, the *PEC* is 1.036, indicating the advantage of low-velocity fluid in enhanced heat transfer. Therefore, the disadvantage of increasing energy consumption at high U_{in} should be considered to improve the economy of heat exchange.

4.2. Effect of row number

To analyze the HTP of the IETBs under different tube row numbers, the fluid domain outlet temperature was recorded for different conditions (VL and FL-heat exchanger) with the U_{in}=0.5 m/s and N=9. The fluid domain temperature field of the *x*-*y* cross section was analyzed, as shown in Fig. 14.

Fig. 14 illustrates the fluid temperature of the different heat exchangers both increased significantly after convective heat transfer, and the wall temperature field can be divided into three parts. The low-temperature part is located at the fore-end, with an average temperature of 293–296 K, the middle part is the sub-high-temperature part, which is around 300 K, and the high-temperature part near the outlet is generally higher than 302 K.

Following the flow direction, the fluid is gradually heated by the IETBs, which makes the temperature gradient on the IETBs section gradually decrease. After the fluid is fully developed, the temperature of the area between the tube bundles increases obviously. Moreover, the deeper the fluid is, the more concentrated the temperature field distribution is.

To analyze the HTP of the IETBs, the h/h_v of the IETBs for different cases was analyzed qualitatively. Fig. 15 manifests the h/h_v with IETBs in different heat exchangers when U_{in} is 0.5 m/s.

It can be seen from Fig. 15,

(1) The h_v of each row is greater than h, which indicates that each IETB has realized enhanced heat transfer.

(2) From IETB 1 to IETB 9, h/h_v represents a general trend of decline. Because the larger the tube number, the farther away the IETB is from the shell inlet. Fig. 16 shows the different cross-sections of turbulent dynamic energy in different heat exchangers. Combined with Fig. 16, it can be seen that after the fluid interacts with the front IETB, the turbulent dynamic energy decreases. This will increase the thermal boundary layer thickness around the rear IETB and reduce the comprehensive HTP of different heat exchangers [20].

(3) FL-heat exchanger has greater h/h_v than the VL-heat exchanger, which is more obvious in the rear IETBs. After calculation, compared with the VL-heat exchanger, h/h_v of the FL–heat exchanger has a maximum increase of 21.12%. This is because the FL-heat exchanger reduces the row spacing, which improves the degree of turbulence on the shell side, especially in the latter part.

Through the research on each IETB HTP, to further analyze the HTP of overall IETBs under different row numbers, the average heat transfer coefficients (h_a/h_{va}) are calculated under different row numbers heat exchangers, as shown in Fig. 17.

As can be drawn from Fig. 17,

(1) For the VL-heat exchanger, h_a/h_{va} decreases as the row number increases. After calculation, while N=6 is increased to N=8, h_a decreases by 14.56%, and h_{va} decreases by 13.85%. This indicates that within the calculation scope of this paper, increasing row number N will weaken the fluid turbulence degree.

(2) For the FL-heat exchanger, the trend of h_a/h_{va} changes differently as the N changes. The increase of row number on the one hand will weaken the turbulence degree, resulting in the decrease of h_a; On the other hand, as the spacing decreases, vortex street shedding is generated after the interaction between shell side fluid and front IETB will more easily act on the back row and enhance its vibration response. Previous studies have shown that under strong vibration conditions, the thermal conductivity is reduced since the boundary layer cannot stately generate. As a result, the h_a/h_{va} of IETBs would improve. When N is increased from 6 to 7, the effect of spacing is greater, so the h_a and h_{av} increase by 2.85% and 2.55%, respectively. After N=7, the reduction of turbulence degree is more significant, resulting in a decrease in h_a/h_{va}.

(3) Compared FL-heat exchanger with the VL-heat exchanger, the smaller the spacing, the greater the h_a/h_{va}. While the spacing in the FL-heat exchanger (H=108 mm) is larger than that VL-heat exchanger (H=90 mm) at N=6, the h_a and h_{va} are reduced by 10.34% and 8.60%, respectively. When N=9, the FL-heat exchanger has a smaller spacing than that at the VL-heat exchanger, so the h_a and h_{va} are increased by 4.13% and 5.22%, respectively. This is consistent with the analysis in conclusion (2).

Through the research on HEP of overall IETBs, to investigate the comprehensive HTP of the heat exchanger under different row numbers, the average heat transfer coefficient per unit pressure drop under vibration $h_{va}/\Delta P$ and *PEC* are calculated for different row numbers, as shown in Fig. 18.

As can be drawn from Fig. 18,

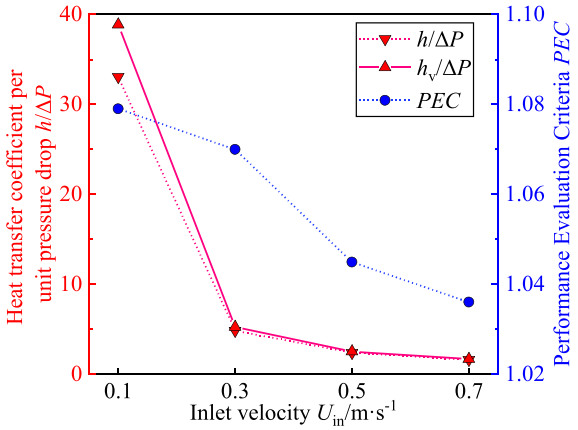

Fig. 13. Influence of U_{in} on $h/\Delta P$ and *PEC*.

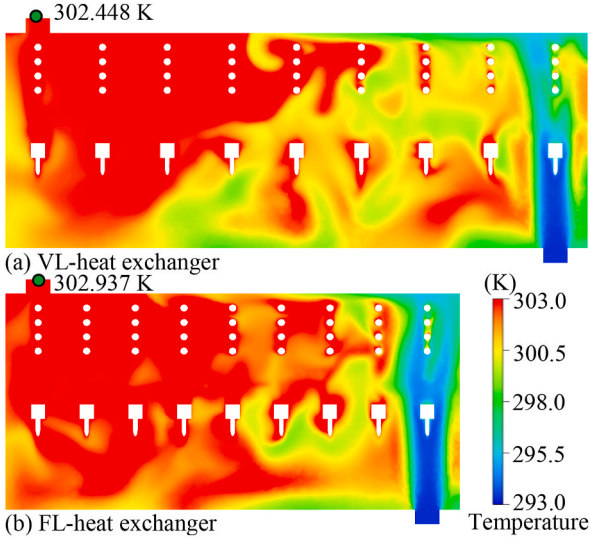

Fig. 14. Temperature field of IETB heat exchanger.

(1) For the VL-heat exchanger, comprehensive HTP decreases gradually with the rising of row number, because the increase of row numbers weakens the turbulent kinetic energy and increases the energy consumption, leading to a significant decrease in comprehensive HTP. From N=7 to N=9, $h_{va}/\Delta P$ and *PEC* decreased by 11.74% and 3.74% respectively.

(2) For the FL-heat exchanger, the comprehensive HTP keeps the same trend as the h_a/h_{va} within the range of calculation in this paper, that is, it has a maximum while N is 7 and then decreases gradually. The reason for the same change trend is that under the condition of the FL-heat exchanger, the inlet and outlet pressure changes little due to the constant flow field length. Between the N=6–8, the ΔP change rate is only 1.75%. Similarly, other variables, such as velocity and density, change little on the whole. Therefore, the changing trend of comprehensive HTP is generally similar to h_a/h_{va}.

(3) Comparing the two categories, the smaller the spacing is, the better comprehensive HTP is. On the one hand, within the calculation examples in this paper, the shell side length is shorter and the energy consumption is lower at low spacing; On the other hand, according to the previous analysis, the h_a/h_{va} is greater at low spacing. Considering the influence of the two parameters, the comprehensive HTP at low spacing is better.

To study the heat exchanger efficiency, the heat transfer per unit volume Q_{vo} is calculated to quantitatively reflect the comprehensive HTP, as shown in Fig. 19.

$$Q_{vo} = \frac{q \cdot S}{V} \tag{12}$$

where where the equation involves the effective heat transfer area (S) and fluid domain volume (V).

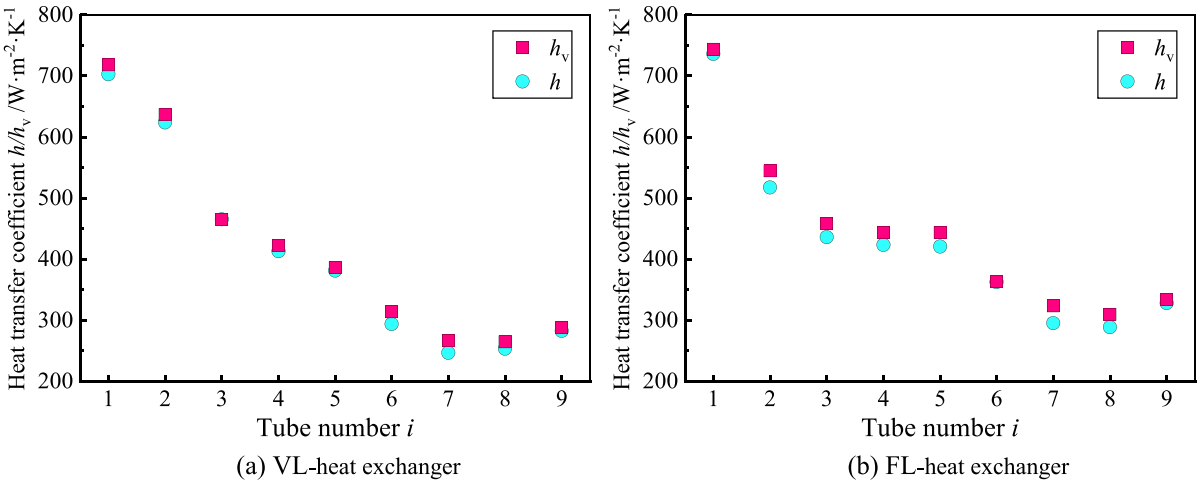

Fig. 15. Heat transfer coefficient h/h_v of IETBs.

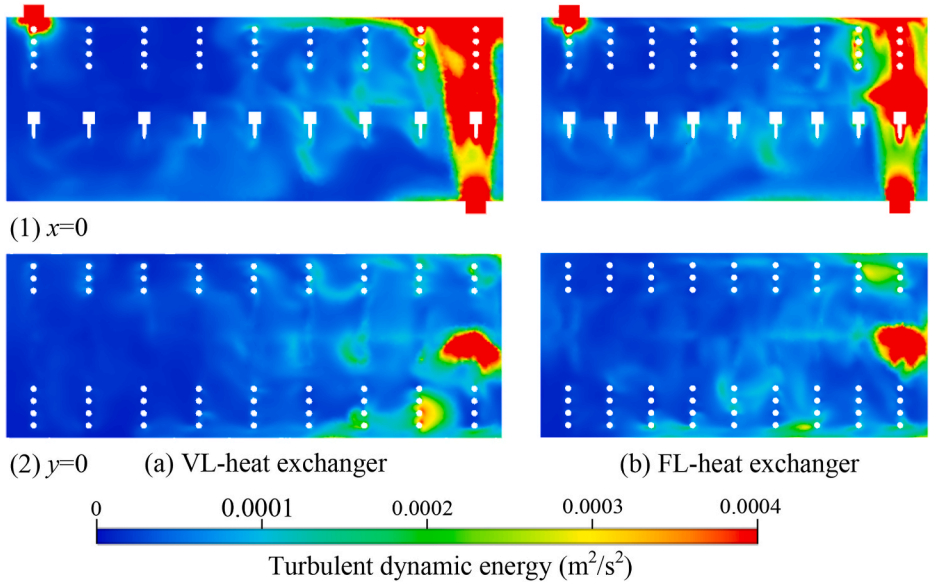

Fig. 16. Turbulent kinetic energy diagram.

It is evident from Fig. 19, Q_{vo} increases with the increase of N, with a small overall change for the VL-heat exchanger. The minimum value is obtained at N=7 (corresponds to the heat exchanger in Ref. [20]). Comparing the maximum and minimum values, the difference between the two is 8.88%. It can be seen that the research in this paper is of guidance in improving the integrated heat transfer performance of heat exchangers in the literature [20]. For the FL-heat exchanger, Q_{vo} increases with the increase of N. While the N=6 increases to N=9, Q_{vo} increases by 86.98%. Comparing the Q_{vo} of the VL-heat exchanger and FL-heat exchanger, it can be found that the method of using fixed shell side length is more practical when increasing the heat exchanger comprehensive HTP by increasing the number of tube rows, which also provides ideas for the optimization method of increasing the heat exchanger comprehensive HTP.

5. Conclusion

Based on the bi-directional fluid-structure interaction calculation method, the effect of U_{in} and row number N on vibration and HTP of the IETB heat exchanger are studied. According to the results above, the key conclusions follow.

(1) The average amplitude of IETBs in different row numbers gradually increases with the rising of U_{in}. The vibration uniformity of the IETBs is better at low U_{in}. Besides, the difference in amplitude among different IETBs becomes larger and larger. And the amplitude in the FL-heat exchanger is generally higher than the VL-heat exchanger. For the VL-heat exchanger, when the row number is increased, the average amplitude decreases gradually. For the FL-heat exchanger, it decreases first and then increases.

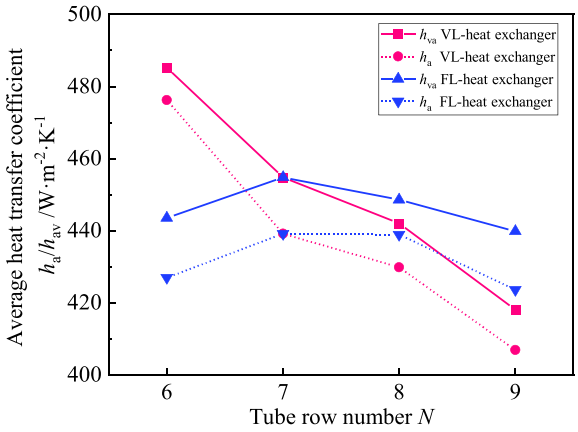

Fig. 17. The effect of row number on the h_a/h_{va}.

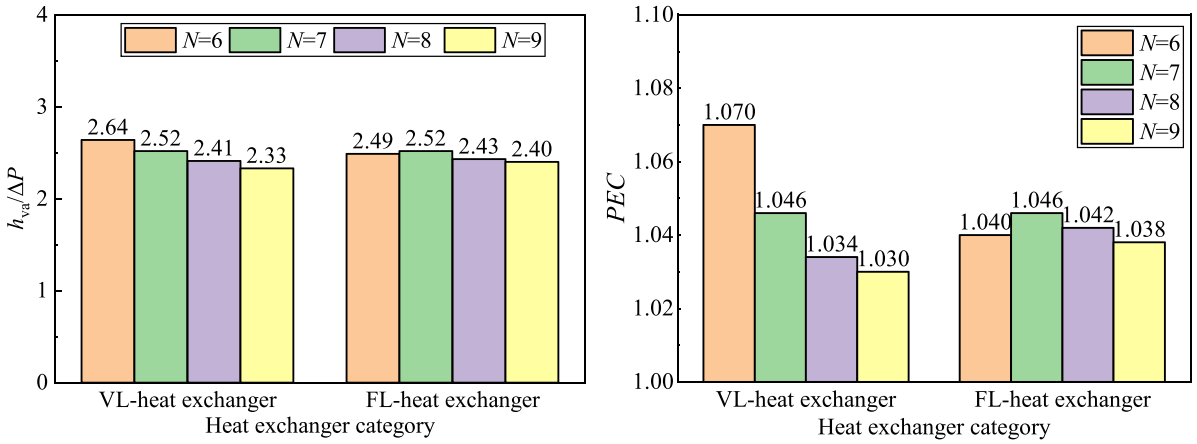

Fig. 18. Comprehensive HTP with different row numbers.

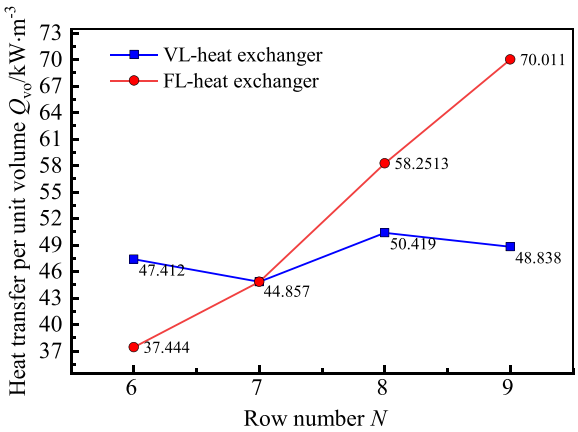

Fig. 19. Q_{vo} with different row numbers.

(2) The average heat transfer coefficient h_a/h_{va} of IETBs is directly proportional to U_{in} and comprehensive HTP decreases gradually with the rising of U_{in}. With the increase of tube number i, the h_a/h_{va} presents a general trend of decline. And h_a/h_{av} in the FL-heat exchanger is generally greater than that VL-heat exchanger. In addition, the h_{va} is always greater than h, which indicates that vibration facilitates the achievement of heat transfer enhancement.

(3) The smaller the spacing, the larger the h_a/h_{va}. While N=6, the FL-heat exchanger spacing (H=108 mm) is larger than that of the VL-heat exchanger (H=90 mm), and h_a and h_{va} decrease by 10.34% and 8.60%, respectively. While N=9, the FL-heat exchanger has a smaller spacing than the VL-heat exchanger, so h_a and h_{va} increase by 4.13% and 5.22%, respectively. It shows that the smaller the spacing between IETBs, the better the comprehensive HTP. By comparing the heat transfer per unit volume, it was determined that the use of fixed shell side length is better in terms of improving the comprehensive HTP by increasing the row numbers in the IETB heat exchanger.

Declaration of competing interest

The authors declare that they have no known competing financial interests or personal relationships that could have appeared to influence the work reported in this paper.

Data availability

The authors do not have permission to share data.

Acknowledgements

This work was supported by National Natural Science Foundation of China (grant number 52175070); Natural Science Foundation of Anhui Province (grant number 1908085ME160); Key Project Foundation of Natural Science Research in Universities of Anhui Province in China (grant number KJ2018A0080); and Anhui Provincial Key Research and Development Project (Grant No. 2022a05020030).

References

[1] M. Mehdi, R.D. Mehdi, T. Davood, et al., Numerical investigation of grooves effects on the thermal performance of helically grooved shell and coil tube heat exchanger, Chin. J. Chem. Eng. 44 (2022) 424–434, https://doi.org/10.1016/j.cjche.2021.05.038.
[2] R. Gugulothu, N. Sanke, et al., Numerical study of heat transfer characteristics in shell-and-tube heat exchanger, Numerical Heat Transfer and Fluid Flow (2018) 375–383, https://doi.org/10.1007/978-981-13-1903-7_43.
[3] R. Gugulothu, N. Sanke, F. Ahmed, et al., Numerical study on shell and tube heat exchanger with segmental baffle, Proceedings of International Joint Conference on Advances in Computational Intelligence (2021) 309–318, https://doi.org/10.1007/978-981-16-0586-4_25.
[4] H. Zheng, R.E. Price, Y. Modarres-Sadeghi, et al., On fatigue damage of long flexible cylinders due to the higher harmonic force components and chaotic vortex-induced vibrations, Ocean Eng. 88 (2014) 318–329, https://doi.org/10.1016/j.oceaneng.2014.06.041.
[5] Y. Gong, J. Zhong, Z.G. Yang, Failure analysis of bursting on the inner pipe of a jacketed pipe in a tubular heat exchanger, Mater. Des. 88 (2010) 4258–4268, https://doi.org/10.1016/j.matdes.2010.04.010.
[6] R. Gugulothu, N. Sanke, S. Nagadesi, et al., Thermal hydraulic performance of helical baffle shell and tube heat exchanger using RSM method, Applied Analysis, Computation and Mathematical Modelling in Engineering 1 (2022) 167–187, https://doi.org/10.1007/978-981-19-1824-7_11.
[7] R. Gugulothu, N. Sanke, Use of segmental baffle in shell and tube heat exchanger for nano emulsions, Heat Transfer 51 (2022) 2645–2666, https://doi.org/10.1002/htj.22418.
[8] L.K. Nitturi, V.K.S. Kapu, R. Gugulothu, Augmentation of heat transfer through passive techniques, Heat Transfer (2023), https://doi.org/10.1002/htj.22877.
[9] L. Cheng, M.C. Tian, G.M. Zhang, et al., Theoretical analysis of complex heat transfer enhancement by flow-induced vibration, J. Eng. Thermophys. 23 (2002) 330–332.
[10] L. Cheng, T. Luan, W. Du, et al., Heat transfer enhancement by flow-induced vibration in heat exchangers, Int. J. Heat Mass Tran. 52 (2009) 1053–1057, https://doi.org/10.1016/j.ijheatmasstransfer.2008.05.037.
[11] K. Yan, P.Q. Ge, W.B. Bi, et al., Vibration characteristics of fluid-structure interaction of conical spiral tube bundle with FEM, J. Hydrodyn. 22 (2010) 121–128, https://doi.org/10.1016/S1001-6058(09)60036-6.
[12] K. Yan, P.Q. Ge, Y.C. Su, et al., Numerical simulation on heat transfer characteristic of conical spiral tube bundle, Appl. Therm. Eng. 31 (2011) 284–292, https://doi.org/10.1016/j.applthermaleng.2010.09.008.
[13] B. Jiang, Analysis on Mechanism of Heat Transfer Enhancement by Vibration and Experimental Research on a New Type of Vibrational Heat Transfer Component, Shandong University, Jinan, PRC, 2010.
[14] J.D. Ji, R.M. Gao, W.Q. Chen, et al., Analysis of vortex flow in fluid domain with variable cross-section and design of a new vortex generator, Int. Commun. Heat Mass Tran. 116 (2020), 104695, https://doi.org/10.1016/j.icheatmasstransfer.2020.104695.
[15] J.D. Ji, W.Q. Chen, R.M. Gao, et al., Research on vibration and heat transfer in heat exchanger with vortex generator, J. Thermophys. Heat Tran. 35 (2020) 164–170, https://doi.org/10.2514/1.T6081.
[16] J.D. Ji, Study on Flow-Induced Vibration of Elastic Tube Bundle with Shell-Side Distributed Pulsating Flow in Heat Exchanger, Shandong University, Jinan, PRC, 2016.
[17] D.R. Duan, P.Q. Ge, W.B. Bi, et al., Numerical investigation on synthetical performance of heat transfer of planar elastic tube bundle heat exchanger, Appl. Therm. Eng. 109 (2016) 295–303, https://doi.org/10.1016/j.applthermaleng.2016.08.070.
[18] D.R. Duan, P.Q. Ge, W.B. Bi, Numerical investigation on heat transfer performance of planar elastic tube bundle by flow-induced vibration in heat exchanger, Int. J. Heat Mass Tran. 103 (2016) 868–878, https://doi.org/10.1016/j.ijthermalsci.2016.11.003.
[19] J.D. Ji, R.M. Gao, B.J. Shi, et al., Improved tube structure and segmental baffle to enhance heat transfer performance of elastic tube bundle heat exchanger, Appl. Therm. Eng. 200 (2022), 117703, https://doi.org/10.1016/j.applthermaleng.2021.117703.
[20] J.D. Ji, J.W. Zhang, F.Y. Li, et al., Numerical research on vibration-enhanced heat transfer of improved elastic tube bundle heat exchanger, Case Stud. Therm. Eng. 33 (2022), 101936. https://10.1016/j.csite.2022.101936.
[21] R. Gugulothu, N. Sanke, F. Ahmed, et al., Numerical investigation of baffle spacing in a shell and tube heat exchanger with segmental baffle, Applied Analysis, Computation and Mathematical Modelling in Engineering 897 (2021) 83–98, https://doi.org/10.1007/978-981-19-1824-7_6.
[22] R. Gugulothu, N. Sanke, Effect of helical baffles and water-based Al2O3, CuO, and SiO2 nanoparticles in the enhancement of thermal performance for shell and tube heat exchanger, Heat Transfer 51 (2022) 3768–3793, https://doi.org/10.1002/htj.22474.

[23] A. Kaleru, S. Venkatesh, N. Kumar, Numerical and experimental study of a shell and tube heat exchanger for different baffles, Heat Transfer 52 (2022) 2186–2206, https://doi.org/10.1002/htj.22780.
[24] A. Kaleru, S. Venkatesh, N. Kumar, Theoretical and numerical study of a shell and tube heat exchanger using 22% cut segmental baffle, Heat Transfer 51 (2022) 7805–7821, https://doi.org/10.1002/htj.22667.
[25] M.R. Salimpour, Heat transfer coefficients of shell and coiled tube heat exchangers, Exp. Therm. Fluid Sci. 33 (2009) 203–207, https://doi.org/10.1016/j.expthermflusci.2008.07.015.
[26] R.L. Webb, Performance evaluation criteria for use of enhanced heat transfer surfaces in heat exchanger design, Int. J. Heat Mass Tran. 24 (1981) 715–726.
[27] G. Lu, G. Zhou, Numerical simulation on performances of plane and curved winglet type vortex generator pairs with punched holes, Int. J. Heat Mass Tran. 102 (2016) 679–690, https://doi.org/10.1016/j.ijheatmasstransfer.2016.06.063.
[28] J.D. Ji, P.Q. Ge, W.B. Bi, Numerical analysis on shell-side flow-induced vibration and heat transfer characteristics of elastic tube bundle in heat exchange, Appl. Therm. Eng. 107 (2016) 544–551, https://doi.org/10.1016/j.applthermaleng.2016.07.018.